Blue Phosphorescent Iridium Complexes with Fluorine-free Main Ligands for Efficient Organic Light-emitting Diodes

Hwa Yong Shin, Seongjin Jeong, Sung Hyun Kim, and Jong-In Hong*

Department of Chemistry, College of Natural Sciences, Seoul National University, Seoul 08826, Korea.
**E-mail: jihong@snu.ac.kr*
Received May 4, 2017, Accepted June 5, 2017, Published online July 14, 2017

Two heteroleptic iridium(III) complexes with fluorine-free pyridylpyrimidine main ligands were designed and synthesized for use as blue phosphorescent emitters in organic light-emitting diodes (OLEDs). Complexes 1 and 2 have a molecular formula of $Ir(C^N)_2(L^X)$, where C^N = 2-tert-butyl-5-(pyridin-2-yl) pyrimidine (b5ppmH) is the main ligand and L^X = picolinic acid (pic) and 2-(1H-tetrazol-5-yl)pyridine (ptz) are ancillary ligands. The thermal, photophysical, and electrochemical properties of these complexes were investigated. Even without electron-withdrawing fluorine substituents, the complexes emitted blue light at 463 and 455 nm with moderate quantum efficiencies (Φ_{PL} = 0.54 and 0.43), respectively. Furthermore, the replacement of the pyridine ring with a pyrimidine ring allowed blue emission without fluorine substituents. An organic light-emitting device fabricated using complex 2 as a dopant and 1,3-bis(N-carbazolyl)benzene (mCP) as a host exhibited a maximum external quantum efficiency of 11.5% and color coordinates of (0.17, 0.26) at 100 cd/m^2.

Keywords: Fluorine-free, Blue phosphorescent OLEDs, Iridium complex, Pyrimidine

Introduction

Over the last three decades, organic light-emitting diodes (OLEDs) have attracted considerable attention because of their potential applications in the next generation flat-panel displays and solid-state lighting sources.[1–4] Phosphorescent OLEDs have attracted more attention than fluorescent OLEDs due to the high quantum yields of iridium- and platinum-based emitters.[5–9] The color coordinates of these materials can also be tuned by ligand substitution, allowing full coverage of the visible wavelength region.[10]

In particular, the efficiencies of green and red phosphor based devices have reached the theoretical limits.[11–13] In contrast, few reports have been made concerning blue phosphorescent emitters that have both high color purity and high brightness, due to their high triplet energies.[14,15] Thus, commercial OLEDs still consist of phosphorescent green/red and fluorescent blue emitters. Consequently, blue emitters are highly desired to overcome this bottleneck in phosphorescent emitter-containing OLEDs. For a complex to emit blue phosphorescence, the energy band gap (E_{gap}) between the lowest unoccupied molecular orbital (LUMO) and highest occupied molecular orbital (HOMO) must be large. The HOMO–LUMO gap can be increased by modifying the main ligand. Generally, two methods are used to produce a large HOMO–LUMO energy band gap. First, the substitution of an electron-withdrawing group on the phenyl ring of the 2-phenylpyridine (ppy) main ligand in tris[2-phenylpyridinato-C2,N]iridium(III), ($Ir(ppy)_3$), which is a widely used green emitter and a general starting material for iridium-based blue dopants, would lower the energy of the HOMO, leading to a blue-shifted emission. In contrast, because the LUMO is localized on the pyridyl ring of the ppy ligand, the introduction of an electron-donating group to the pyridyl ring destabilizes the LUMO energy level. Additionally, replacing the phenyl ring with other electron-deficient heterocyclic rings such as pyridine,[16,17] triazole,[18] or pyrimidine[19] provides an alternative approach, and ligands containing these ring systems show blue-shifted emissions relative to that of ppy ligands due to the larger π–π^* energy band gap. The former strategy is the most popular way to realize deep blue emissions with iridium complexes. For example, Kim *et al.* used electron-withdrawing heptafluoropropyl[20] and perfluoro carbonyl[21] substitution at the phenyl ring of ppy ligands. These complexes exhibit deep blue emissions at 451 and 447 nm, respectively. Other research groups have used (2,4-difluoro-3-trifluoromethylphenyl) pyridine and its derivatives[22,23] to induce deep blue emission. However, the use of fluorine substitution to induce deep blue emission severely affects thermal stability and shortens device lifetime.[24] According to Sivasubramaniam *et al.*, defluorination occurs during sublimation and device operation.[25] Therefore, blue-emitting iridium complexes that do not contain a fluorine moiety are required to achieve longer lifetimes and stable operation.

In this paper, we report fluorine-free iridium complexes for use as blue dopants for phosphorescent OLEDs. We used the strong field ligand 2-tert-butyl-5-(pyridin-2-yl) pyrimidine (b5ppmH) as a fluorine-free main ligand. Using

this ligand, we synthesized complex 1, which has a picolinate ancillary ligand (pic), to investigate the effect of the b5ppmH main ligand on the emission wavelength compared to a representative blue emitter, iridium(III)bis(4,6-(difluorophenyl) pyridinato-N,C2′)picolinate (FIrpic). Additionally, complex 2 with 2-(1H-tetrazol-5-yl)pyridine (ptz) as an ancillary ligand was synthesized to induce further blue emission shifts. The two complexes have good thermal properties and quantum efficiencies. Moreover, they have low color coordinate y compared to that of FIrpic. The OLED device based on iridium complex 2 with a fluorine-free structure exhibited a maximum external quantum efficiency of 11.5% and a color coordinates of (0.17, 0.26).

Results and Discussion

Synthesis. The synthetic scheme for complexes 1 and 2 is shown in Scheme 1. 2-tert-Butyl-5-(pyridin-2-yl)pyrimidine (b5ppmH) was synthesized through the Stille coupling reaction between with 5-bromo-2-tert-butylpyrimidine and 2-(tributylstannyl)pyridine. Dichloro-bridged iridium dimers were obtained by heating a mixture of b5ppmH and $IrCl_3 \dot{c} nH_2O$ at reflux in 2-methoxyethanol. Complexes 1 and 2 were prepared by adding ancillary ligands to iridium dimers in the presence of Na_2CO_3. All synthesized complexes were characterized by nuclear magnetic resonance (NMR) spectroscopy and high-resolution mass spectra (HRMS). Details are presented in the Experimental section.

Thermal Stability. To investigate the thermal stabilities of each iridium complex, thermal gravimetric analysis (TGA) was carried out. Generally, materials that have decomposition temperature above 300°C can be vacuum deposited without degradation, during manufacturing OLEDs.[26] The decomposition temperature of the complexes was defined as the temperature at which 5% weight loss occurs. As shown in Figure 1, complexes 1 and 2 have decomposition temperatures of 339 and 356°C, respectively. Such high thermal stabilities are attributed to the fluorine-free structure, which enables each complex to be deposited by thermal evaporation. In addition, this material property guarantees good morphological stability and stable operation of the devices.

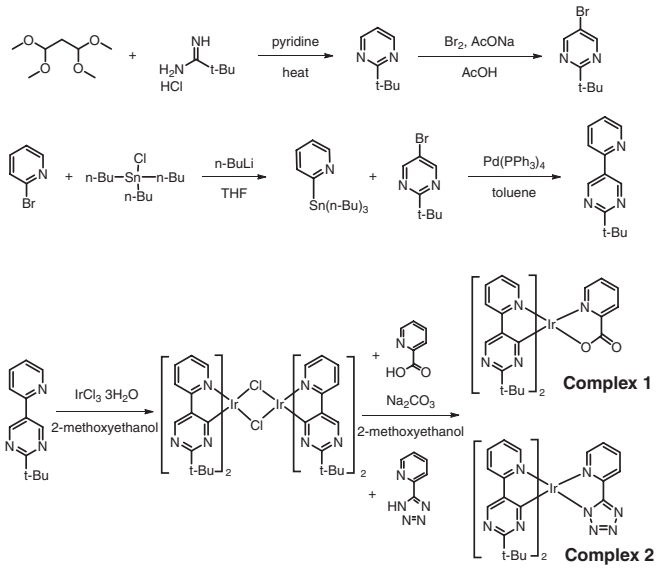

Scheme 1. Synthetic routes of a main ligand and complexes 1 and 2.

X-ray Crystallography. The molecular structures of the synthesized Ir(III) complexes 1 and 2 were determined by single-crystal x-ray structure analysis. The structures of each complex are shown in Figure 2. Selected bond lengths are summarized in Table 1, and the crystal structure data in Table S1 (Supporting Information). The Ir–N bond distances in each complex are ca. 2.043–2.199 Å. The Ir–N (pyrimidine) bond distances in each complex are similar (2.043–2.063 Å), which are shorter than Ir–N bond distances at each ancillary ligand (2.144–2.199 Å). The Ir–C bond distances (1.967–1.995 Å) in each complex are shorter than other bond distances, which are attributed to the trans-influence of opposite N or O atoms in ancillary ligands.

Photophysical Properties. The absorption and phosphorescent emission spectra of each iridium complex were measured in dichloromethane (10^{-5} M) at room temperature, and are shown in Figure 3. All photophysical data are summarized in Table 2. In the absorption spectra, each complex has similar spectral patterns. An intense absorption in the range of 240 to 270 nm is attributed to the allowed ligand-centered (^{1}LC) transition of cyclometalated ligands. The absorption bands at around 350 nm are attributed to the allowed metal-to-ligand charge transfer (^{1}MLCT) transition. A weak absorption in the longer wavelength region, greater than 380 nm, is assigned to a mixture of forbidden ligand-centered transitions and metal-to-ligand charge transfer transitions (^{3}LC and ^{3}MLCT). When excited at 340 nm radiation, each complex showed strong blue emission with the first peak maxima being located at 463 and 455 nm for complexes 1 and 2, respectively. Each complex exhibited significantly blue-shifted emissions compared to the representative sky-blue emitter complex, FIrpic. The blue-shifted emissions can be attributed to the replacement of the phenyl group with a pyrimidine ring in each complex, leading to higher energy π–π* ligand transitions. In addition, the replacement of pic by ptz ancillary ligand caused a hypsochromic shift of about 8 nm for complex 2. This indicates that blue-shifted emission is strongly dependent on the nature of the ancillary ligands. The ptz ligand of complex 2 has a stronger electron-withdrawing ability than the picolinate ligand of complex 2. Each complex has well-structured emission profiles at room temperature. According to previous studies,[27] the lowest excited triplet states (T_1) of complexes that have dominant ^{3}LC characteristics mixed with ^{3}MLCT contributions shows sharp and well-structured emission features. On the other

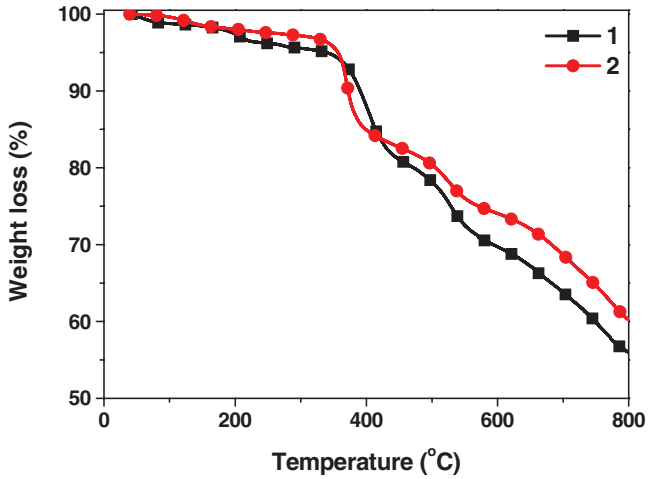

Figure 1. TGA curves of complexes 1 and 2.

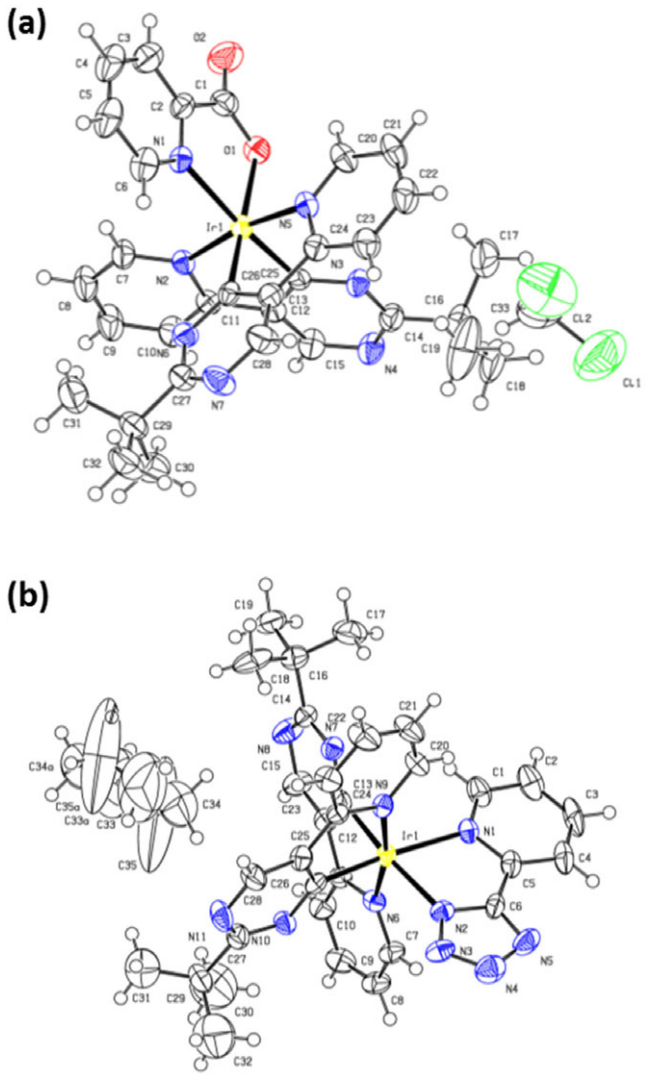

Figure 2. ORTEP diagrams of (a) complex 1 (CCDC 1546119) and (b) complex 2 (CCDC 1546120).

Table 1. Selected bond distances (Å) of complexes 1 and 2.

Bond distance (Å)			
Complex 1		Complex 2	
Ir—N1	2.151	Ir—N1	2.199
Ir—N2	2.043	Ir—N2	2.144
Ir—N5	2.052	Ir—N6	2.064
Ir—C13	1.984	Ir—N9	2.049
Ir—C26	1.967	Ir—C13	1.993
Ir—O1	2.159	Ir—C26	1.995

hand, the emission of complexes with the dominant ^{3}MLCT characteristic in the lowest triplet state exhibits broad and structureless feature. The phosphorescence of each complex originated predominantly from the π–π* characteristics of the complexes, with a minor contribution from the MLCT characteristics. The low-temperature phosphorescence spectra at 77 K also support our analysis that the emissions mainly originate from ligand-centered transitions. The photoluminescence spectra at 77 K contain highly resolved vibrational features along with a slightly blue-shifted emission, compared to the room temperature PL spectra. T_1

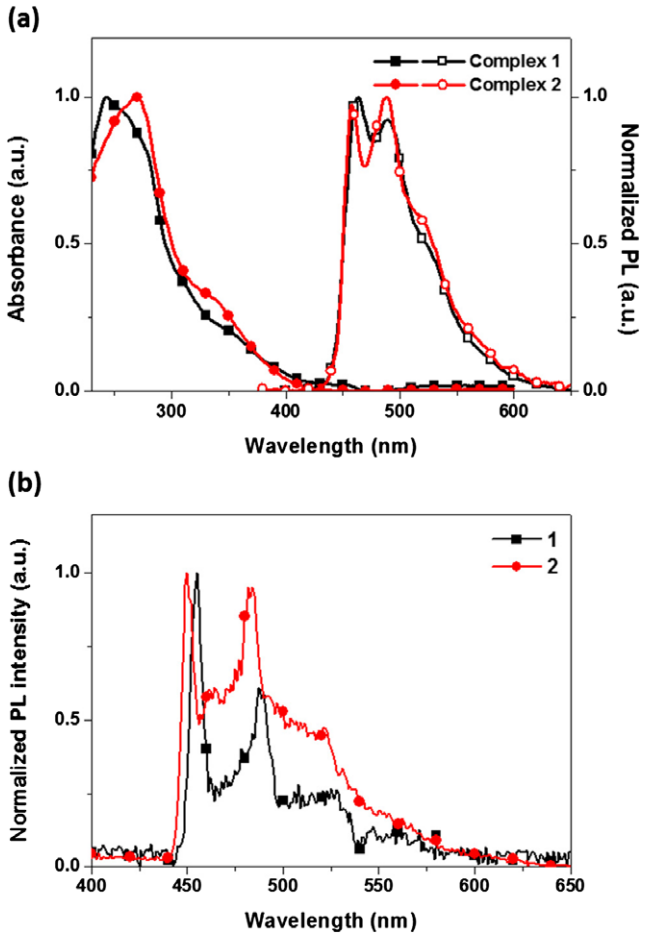

Figure 3. (a) UV–Vis absorption and photoluminescence (PL) spectra of complexes 1 and 2 at room temperature. (b) PL spectra of complexes 1 and 2 at 77 K.

Table 2. Photophysical and electrochemical properties of complexes 1 and 2.

Complex	λ_{abs} (nm)[a]	$\lambda_{em,\ RT}$ solution[a]/ film[b] (nm)	$\lambda_{em,\ 77K}$[c] (nm)	Φ[d]	τ_{obs}[e] (μs)	k_r[f] (10^5 s^{-1})	k_{nr}[f] (10^5 s^{-1})	E_T (eV)	E_{gap} (eV)	HOMO/ LUMO[g] (eV)
Complex 1	244, 354	463, 490/465, 493	455	0.54	2.53	2.13	1.82	2.73	2.95	−5.51/−2.56
Complex 2	249, 337	455, 485 / 459, 486	450	0.46	0.768	5.99	7.03	2.76	3.17	−5.91/−2.74

[a] Measured in CH_2Cl_2 at [M] = 1.0×10^{-5} M.
[b] Doped into mCP at 10 wt %.
[c] Measured in frozen 2-methyltetrahydrofuran matrix at [M] = 1.0×10^{-5} M.
[d] Phosphorescence quantum efficiency was measured in CH_2Cl_2 relative to FIrpic (Φ = 0.60).
[e] Measured in toluene at [M] = 1.0×10^{-4}.
[f] Calculated by equations; $k_r = \Phi/\tau_{obs}$, $k_{nr} = (1-\Phi)/\tau_{obs}$.
[g] HOMO was estimated from their corresponding oxidation potential obtained from CV experiments, LUMO = HOMO + E_{gap}.

energy of each complex was estimated to be 2.73 and 2.76 eV for complexes 1 and 2, respectively. In the film state, each complex showed redshifts of about 2–4 nm due to aggregation and intermolecular interactions of the complexes (Figure S1). The quantum yields (Φ) were estimated to be 0.54 for complex 1 and 0.46 for complex 2, using FIrpic as a reference (Φ = 0.60) (Table 2). In addition, quantum yields of the two complexes measured on solid phase with integrating sphere were 0.43 and 0.28, respectively. Meanwhile, we investigated the decay rate characteristics through time-resolved phosphorescence lifetime measurements in solution and solid state. The observed lifetimes of complexes 1 and 2 were 2.53 and 0.768 μs in dichloromethane solution, respectively, and 3.34 and 2.85 μs in an mCP film, respectively. These values suggest that the two complexes are suitable for use as emitters for high-efficiency OLEDs.

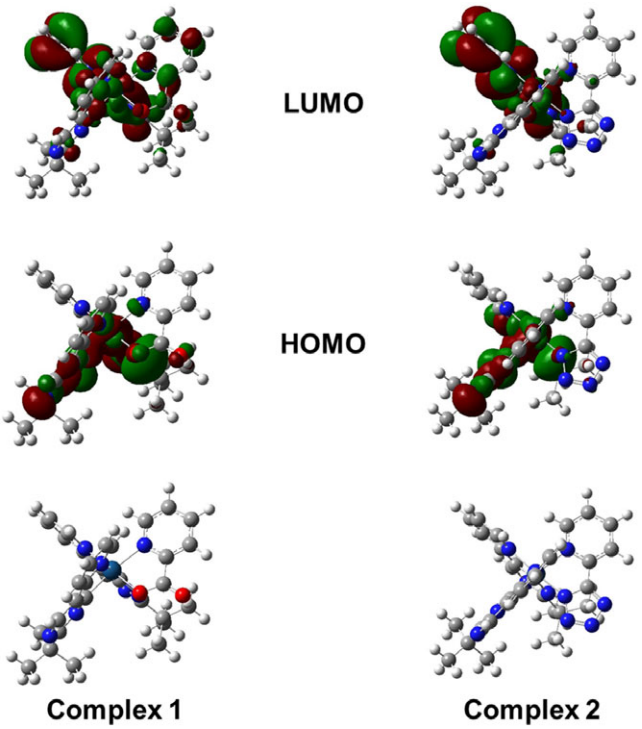

Figure 4. DFT calculated frontier molecular orbitals of complexes 1 and 2.

Electrochemical Properties. To investigate the electrochemical properties of complexes 1 and 2, cyclic voltammetry (CV) measurements were carried out, and the results were used to determine the HOMO energies of the complexes. The HOMO energy was calculated from the onset of the oxidation potentials with respect to the energy level of ferrocene. As shown in Figure S3, each compound exhibited irreversible oxidation in dichloromethane at room temperature. Oxidation potentials (E_{ox}) of complexes 1 and 2 were 0.98 and 1.38 eV, respectively. The HOMO energies of the compounds were calculated to be −5.51 and −5.91 V for complexes 1 and 2, respectively. The energy band gaps (E_{gap}) were obtained from absorption onset to be 2.95 and 3.17 eV for complexes 1 and 2. The LUMO energies were estimated using the following equation E_{LUMO} = (E_{HOMO} + E_{gap}) eV. Complex 2, which has more electron-deficient ancillary ligands, appeared to have more stabilized, lower energy HOMOs compared to complex 1 with a picolinate ancillary ligand. As the electron-withdrawing ability of ancillary ligands increases, the HOMO is stabilized to a greater extent. The effect of stabilization on the HOMO is greater than that on the LUMO, causing the energy band gaps of complex 2 to increase. Therefore, complex 2 is expected to have color coordinates corresponding to deeper blue emission compared to those of complex 1.

Theoretical Calculations. To evaluate the energy levels and orbital electron density distributions of the HOMOs and LUMOs in each iridium complex, density functional theory (DFT) calculations were carried out. Significant frontier molecular orbitals for each complex are shown in Figure 4. The optimized geometries are shown, and the geometry around the Ir atom is that of a distorted octahedron. The HOMOs of each complex are mainly localized on the iridium cation and the pyrimidine ligand, involving the d-orbitals of the metal and π orbitals of the cyclometalated ligands. The ptz ancillary ligand causes the HOMO energy of complex 2 to decrease compared to that of complex 1. The LUMO orbitals of each complex are localized at similar positions, i.e., the π* orbitals of pyridine and

pyrimidine in the cyclometalated ligands, except for contribution from picolinate in complex 1. Therefore, transitions are mostly governed by the LC characteristics of the complexes. This interpretation coincides with that derived from the above-mentioned emission profiles.

Electroluminescent Properties. To evaluate the electroluminescent (EL) characteristics, devices were fabricated using complex 2 and FIrpic as dopant materials, respectively, because complex 2 exhibited the deeper blue emission with moderate quantum efficiency than complex 1. The device fabricated using FIrpic as the dopant was used as a reference. The structure of blue EL device was as follows: ITO/NPB (20 nm)/TAPC (20 nm)/mCP:complex 2 or FIrpic (10 wt %) (30 nm)/TSPO1 (5 nm)/TPBi (45 nm)/LiF (1 nm)/Al (100 nm). The device configuration and energy levels of each organic layer are shown in Figure 5(b) inset. NPB and TAPC were used as hole injecting and transporting layers. Because the gap between HOMO levels of NPB and mCP are large, TAPC was inserted to facilitate hole injection. TSPO1 was used as hole and/or exciton blocking layer because of its high triplet energy (E_T = 3.36 eV). TPBi was inserted as an electron-transporting layer. mCP was selected as a host material because its HOMO and LUMO levels are well matched with those of complex 2. The device performances are shown in Figure 5 and summarized in Table 3. Current density–voltage–luminescence (J–V–L) curves are shown in Figure 5(a), and the turn-on voltage was found to be 4.4 V. At a practical brightness of 100 cd/m^2, the driving voltage was 5.9 V and the external quantum efficiency was 11.1%. The maximum external quantum efficiency was 11.5%, as shown in Figure 5(b). EL spectra at various voltages are illustrated in Figure 5(c). The maximum emission appeared at 455 nm, and no additional emissions from the host or intimate layers were detected, illustrating the high recombination efficiency between holes and electrons in the emitting layer. The emission profiles were mostly unchanged as the driving voltage increased. This stable emission profile on increasing driving voltage indicates that the device can be stably operated. The color coordinates were (0.17, 0.26) at 100 cd/m^2, as shown in Figure 5 (c) inset. The OLED device fabricated using complex 2, which has no fluorine substituents, has a lower *y*-coordinate value compared to that of the FIrpic-based OLED device (0.14, 0.33).[28] Therefore, we believe that devices derived from complex 2 will show better long-term stability than FIrpic-based devices.

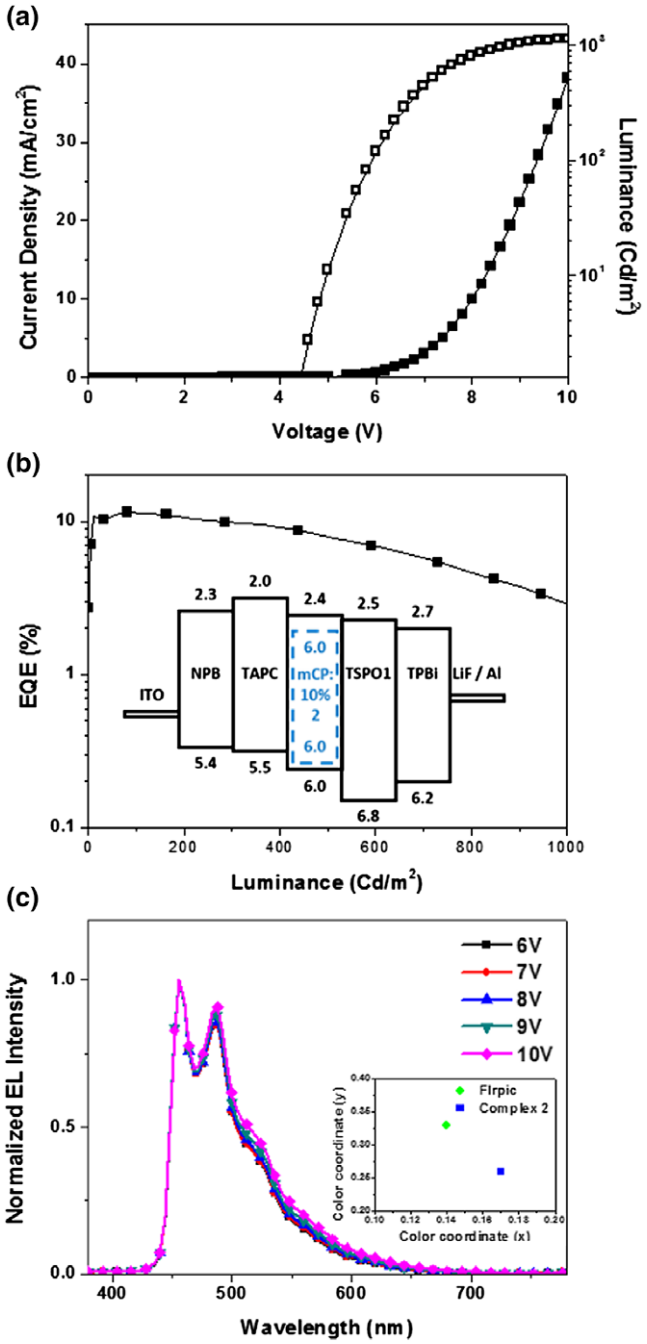

Figure 5. (a) J–V–L characteristics. (b) External quantum efficiency vs. luminescence. Inset: Device configuration and energy level diagram. (c) Electroluminescence spectrum with increasing driving voltage. Inset: Color coordinates for FIrpic and complex 2.

Conclusion

In summary, we designed and synthesized fluorine-free blue phosphorescent iridium complexes. Each complex shows blue-shifted emissions compared to the representative blue dopant FIrpic, with comparable quantum efficiencies. The blue-shifted emission arises from the replacement of the pyridine ring with a pyrimidine ring in the cyclometalated ligands. By selecting appropriate ancillary ligands for complexes 1 and 2, emissions occurred at shorter wavelengths. The OLED device based on complex 2 as an emitter has an EL maximum at 455 nm. A maximum external quantum efficiency of 11.5 % at 5.9 V and color coordinates of (0.17, 0.26) at 100 cd/m^2 were obtained when complex 2 was used as an emitter in the OLED device. The color coordinates are comparable with that of the FIrpic-

Table 3. EL performances of the device using complex 2 as a dopant.

	Current efficiency (cd/A)	Power efficiency (lm/W)	EQE (%)	EL_{max} (nm)	CIE (*x*, *s*)
Device	18.65[a], 19.17[b]	9.95[a], 10.38[b]	11.1[b], 11.5[b]	456[a]	(0.17, 0.26)[a]

[a] At 100 cd/m^2.
[b] Maximum value.

based device. Furthermore, it does not contain fluorine, thus increasing its stability under processing conditions. On further optimization of the device structure, we anticipate that better device performance can be attained with these fluorine-free heteroleptic iridium complexes.

Experimental

Materials and Methods. All reactions were performed under a N_2 atmosphere, and solvents were distilled from the appropriate drying agents before use. Commercially available reagents were purchased from Aldrich and Alfa and used without further purification. ^{1}H and ^{13}C NMR spectra were recorded with a Bruker Avance DPX-300 (Billerica, MA, USA) in $CDCl_3$. UV–Vis absorption spectra were measured by Beckman Coulter DU-650 (Brea, CA, USA) at room temperature. Emission spectra were recorded on Jasco FP-6500 (Tokyo, Japan) at room temperature in dichloromethane. Low-temperature phosphorescence spectra were obtained using a Jasco FP-6500 in 2-methyltetrahydrofuran at liquid nitrogen temperature. Quantum yield measurements were carried out at room temperature in a degassed dichloromethane solution using FIrpic as a reference. Solid phase photoluminescence quantum efficiencies were measured using an integrating sphere (600 diameter, Lasphere Co. (North Sutton, NH, US)). Time-resolved phosphorescence lifetime measurements were performed using the time correlated single photon counting (TCSPC) technique with a FluoTime200 spectrometer (PicoQuant (Berlin, Germany)) equipped with a NanoHarp 300 TCSPC board (PicoQuant) and a PMA182 photomultiplier (PicoQuant). The excitation source was a 342-nm picosecond-pulsed diode laser (PicoQuant, PLS340) driven by a PDL800-D driver (PicoQuant). Mass spectra were measured by JMS-600 W operating in fast atom bombardment (FAB) mode. Cyclic voltammetry was performed using a CHI650B electrochemical workstation (CH Instruments). Measurements were made using a three-electrode electrochemical cell. A 0.1 M tetrabutylammonium perchlorate solution in dichloromethane was used as the electrolyte, and the scan rate was 0.1 V/s. All measurements were carried out at room temperature. A glassy carbon electrode, platinum wire, and Ag/AgCl were used as working, counter, and reference electrodes, respectively. Ferrocene was used as the internal standard.

Synthesis of Ligands. 2-tert-Butylpyrimidine,[29] 5-bromo-2-tert-butylpyrimidine,[30] and 2-tert-butyl-5-(pyridin-2-yl) pyrimidine[31] were synthesized via reported procedures. Ancillary ligands were also prepared in several short steps.[32,33]

General Synthesis of Iridium Complexes. A mixture of $IrCl_3$ċnH_2O (0.19 g, 0.55 mmol, 0.5 equiv.) and b5ppmH (0.23 g, 1.1 mmol, 1 equiv) in 2-methoxyethanol (40 mL) was refluxed for 24 h. After cooling to room temperature, 2-picolinic acid (0.17 g, 1.4 mmol, 1.2 equiv) and sodium carbonate (0.6 g, 5.5 mmol, 5 equiv) were added. The mixture was then refluxed for 4 h. The solvent was removed *in vacuo*. The residue was suspended in water and then twice extracted with ethyl acetate. The combined organic layers were dried over sodium sulfate and evaporated under reduced pressure. The crude product was chromatographed using DCM-methanol as the eluent.

(b5ppm)$_2$Ir(pic) (1). Yellow solid, yield: 23%. ^{1}H NMR (300 MHz, $CDCl_3$): δ (ppm) 8.87 (d, *J* = 5.7 Hz, 1H), 8.45–8.39 (m, 3H), 8.00 (t, *J* = 7.7 Hz, 1H), 8.02–7.78 (m, 5H), 7.64 (d, *J* = 2.8 Hz, 1H), 7.48 (t, *J* = 6.9 Hz, 1H), 7.27 (t, *J* = 5.7 Hz, 1H), 7.08 (t, *J* = 6.3 Hz, 1H), 1.14 (s, 9H), 1.05 (s, 9H), ^{13}C NMR (75 MHz, $CDCl_3$): δ (ppm) 180.5, 179.1, 175.4, 174.8, 172.4, 164.4, 163.1, 151.8, 150.2, 149.0, 148.3, 146.8, 146.7, 138.4, 137.7, 137.5, 136.9, 136.7, 128.4, 128.3, 122.8, 122.6, 118.4, 117.9, 39.1, 38.9, 29.5, 29.4. HRMS (FAB) calc'd [M + H] + =740.2319, observed = 740.2327.

(b5ppm)$_2$Ir(ptz) (2). Yellow solid, yield: 18%. ^{1}H NMR (300 MHz, $CDCl_3$): δ (ppm) 8.53–8.48 (m, 3H), 8.02 (t, *J* = 6.6 Hz, 1H), 7.85–7.74 (m, 6H), 7.63 (d, *J* = 5.6 Hz, 1H), 7.35 (t, *J* = 6.1 Hz, 1H), 7.09–6.98 (m, 2H), 1.15 (s, 9H), 1.08 (s, 9H). ^{13}C NMR (75 MHz, $CDCl_3$): δ (ppm) 183.9, 178.5, 175.9, 175.1, 163.9, 163.8, 163.3, 151.3, 149.8, 149.5, 149.2, 147.2, 147.1, 139.3, 137.7, 137.6, 137.2, 136.2, 125.9, 123.3, 123.1, 122.7, 118.6, 118.3, 39.2, 39.0, 29.5, 29.4. HRMS (FAB) calc'd [M + H] + = 764.2544, observed = 764.2551.

Thermal Analysis. The thermal properties of each iridium complex were characterized by thermogravimetric (T_g) measurements. Decomposition temperatures (T_d) were measured using a Q-5000 IR. TGA measurements were performed at 10°C/min under a nitrogen atmosphere.

X-ray Diffraction Analysis. The crystal structures were determined by single-crystal diffractometer at the Western Seoul Center of Korea Basic Science Institute. A yellow block-shaped crystal (0.15 × 0.11 × 0.08 mm^3) was picked up with paraton oil and mounted on a Bruker D8 Venture PHOTON 100 CMOS diffractometer (Rheinstetten, Germany) equipped with a graphite-monochromated Mo Kα (λ = 0.71073 Å) radiation source and a nitrogen cold

stream (−50°C). Data collection and integration were performed with SMART (Bruker, 2012) and SAINT (Bruker, 2012).[34] Absorption correction was performed by multi-scan method implemented in SADABS.[35] The structure was solved by direct methods and refined by full-matrix least-squares on F^2 using SHELXTL.[36] All the non-hydrogen atoms were refined anisotropically, and hydrogen atoms were added to their geometrically ideal positions.

Computational Method. All calculations were performed using Gaussian 09. The geometry optimization of the ground state using DFT was carried out using B3LYP functional with 6-31G(d) basis sets on all atoms except for Ir, for which the LanL2DZ effective core potential and associated valence basis were used.

OLED Fabrication and Measurement. Patterned indium-tin-oxide (ITO)-coated glass substrates with a sheet resistance of 15 Ω per square were washed with distilled water and isopropyl alcohol and sonicated. Then, the substrate was dried in a vacuum oven. UV treatment for 10 min was carried out before vacuum deposition. Organic light-emitting devices were fabricated by high vacuum (2×10^{-6} torr) thermal evaporation. N,N′-Bis(naphthalen-1-yl)-N,N′-bis(phenyl) benzidine (NPB), 4,4′-cyclohexylidenebis[N,N-bis(4-methyl phenyl)benzenamine] (TAPC), 1,3-bis(N-carbazolyl)benzene (mCP), diphenyl-4-triphenylsilylphenyl-phosphine oxide (TSPO1), and 2,2′,2″-(1,3,5-benzinetriyl)-tris(1-phenyl-1-H-benzimidazole) (TPBi) were purchased from commercial sources and used without further purification. The electroluminescent properties were evaluated using a PR-650 SpectraScan SpectraColorimeter as a source meter. Current–voltage-luminescence characteristics were recorded with a programmable sourcemeter equipped with current and voltage sources (Keithley 2400; Keithley, Cleveland, OH, USA).

Acknowledgments. This research was supported by the National Research Foundation (No. 2013R1A1A2074468) funded by the MSIP, and the Industrial Strategic Technology Development Program (No. 10042412), funded by the Ministry of Trade, Industry and Energy. This work was supported by Samsung Display Co., Ltd.

Supporting Information. Additional supporting information is available in the online version of this article.

References

1. B. W. D'Andrade, S. R. Forrest, *Adv. Mater.* **2004**, *16*, 1585.
2. M. A. Baldo, D. F. O'Brien, Y. You, A. Shoustikov, S. Sibley, M. E. Thompson, S. R. Forrest, *Nature* **1998**, *395*, 151.
3. M. A. Baldo, M. E. Thompson, S. R. Forrest, *Nature* **2000**, *403*, 750.
4. J. H. Burroughes, D. D. C. Bradley, A. R. Brown, R. N. Marks, K. Mackay, R. H. Friend, P. L. Burn, A. B. Holmes, *Nature* **1990**, *347*, 539.
5. C. H. Chen, F. I. Wu, Y. Y. Tsai, C. H. Cheng, *Adv. Funct. Mater.* **2011**, *21*, 3150.
6. G. J. Zhou, Q. Wang, C. L. Ho, W. Y. Wong, D. G. Ma, L. X. Wang, *Chem. Commun.* **2009**, *45*, 3574.
7. A. Tsuboyama, H. Iwawaki, M. Furugori, T. Mukaide, J. Kamatani, S. Igawa, T. Moriyama, S. Miura, T. Takiguchi, S. Okada, M. Hoshino, K. Ueno, *J. Am. Chem. Soc.* **2003**, *125*, 12971.
8. J. Lee, H. F. Chen, T. Batagoda, C. Coburn, P. I. Djurovich, M. E. Thompson, S. R. Forrest, *Nat. Mater.* **2016**, *15*, 92.
9. A. B. Tamayo, B. D. Alleyne, P. I. Djurovich, S. Lamamsky, I. Tsyba, N. N. Ho, R. Bau, M. E. Thompson, *J. Am. Chem. Soc.* **2003**, *125*, 7377.
10. Y. Chi, P. T. Chou, *Chem. Soc. Rev.* **2010**, *39*, 638.
11. B. Liang, C. Y. Jiang, Z. Chen, X. J. Zhang, H. H. Shi, Y. Cao, *J. Mater. Chem.* **2006**, *16*, 1281.
12. K. Y. Lu, H. H. Chou, C. H. Hsieh, Y. H. O. Yang, H. R. Tsai, H. Y. Tsai, L. C. Hsu, C. Y. Chen, I. C. Chen, C. H. Cheng, *Adv. Mater.* **2011**, *23*, 4933.
13. L. X. Xiao, Z. J. Chen, B. Qu, J. X. Luo, S. Kong, Q. H. Gong, J. J. Kido, *Adv. Mater.* **2011**, *23*, 926.
14. Y. C. Chiu, J. Y. Hung, Y. Chi, C. C. Chen, C. H. Chang, C. C. Wu, Y. M. Cheng, Y. C. Yu, G. H. Lee, P. T. Chou, *Adv. Mater.* **2009**, *21*, 2221.
15. C. H. Yang, Y. M. Cheng, Y. Chi, C. J. Hsu, F. C. Fang, K. T. Wong, P. T. Chou, C. H. Chang, M. H. Tsai, C. C. Wu, *Angew. Chem. Int. Ed.* **2007**, *46*, 2418.
16. J. Lee, H. Park, K. M. Park, J. Kim, J. Y. Lee, Y. Kang, *Dyes Pigments* **2015**, *123*, 235.
17. S. J. Lee, K. M. Park, K. Yang, Y. Kang, *Inorg. Chem.* **2009**, *48*, 1030.
18. C. H. Chang, C. L. Ho, Y. S. Chang, I. C. Lien, C. H. Lin, Y. W. Yang, J. L. Liao, Y. Chi, *J. Mater. Chem. C* **2013**, *1*, 2639.
19. T. Duan, T. K. Chang, Y. Chi, J. Y. Wang, Z. N. Chen, W. Y. Hung, C. H. Chen, G. H. Lee, *Dalton Trans.* **2015**, *44*, 14613.
20. J. B. Kim, S. H. Han, K. Yang, S. K. Kwon, J. J. Kim, Y. H. Kim, *Chem. Commun.* **2015**, *51*, 58.
21. S. Lee, S. O. Kim, H. Shin, H. J. Yun, K. Yang, S. K. Kwon, J. J. Kim, Y. H. Kim, *J. Am. Chem. Soc.* **2013**, *135*, 14321.
22. H. J. Park, J. N. Kim, H. J. Yoo, K. R. Wee, S. O. Kang, D. W. Cho, U. C. Yoon, *J. Org. Chem.* **2013**, *78*, 8054.
23. S. Takizawa, H. Echizen, J. Nishida, T. Tsuzuki, S. Tokito, Y. Yamashita, *Chem. Lett.* **2006**, *35*, 748.
24. R. Seifert, I. R. de Moraes, S. Scholz, M. C. Gather, B. Lussem, K. Leo, *Org. Electron.* **2013**, *14*, 115.
25. V. Sivasubramaniam, F. Brodkorb, S. Hanning, H. P. Loebl, V. van Elsbergen, H. Boerner, U. Scherf, M. Kreyenschmidt, *J. Fluorine Chem.* **2009**, *130*, 640.
26. N. Jung, E. Lee, J. Kim, H. Park, K. M. Park, Y. Kang, *Bull. Korean Chem. Soc.* **2012**, *33*, 183.
27. J. Li, P. I. Djurovich, B. D. Alleyne, M. Yousufuddin, N. N. Ho, J. C. Thomas, J. C. Peters, R. Bau, M. E. Thompson, *Inorg. Chem.* **2005**, *44*, 1713.
28. J. K. Bin, N. S. Cho, J. I. Hong, *Adv. Mater.* **2012**, *24*, 2911.
29. T. S. Wang, I. S. Cloudsdale, *Synth. Commun.* **1997**, *27*, 2521.
30. R. G. Pews, *Heterocycles* **1990**, *31*, 109.
31. C. H. Chang, Z. J. Wu, C. H. Chiu, Y. H. Liang, Y. S. Tsai, J. L. Liao, Y. Chi, H. Y. Hsieh, T. Y. Kuo, G. H. Lee,

H. A. Pan, P. T. Chou, J. S. Lin, M. R. Tseng, *ACS Appl. Mater. Interfaces* **2013**, *5*, 7341.
32. E. Orselli, G. S. Kottas, A. E. Konradsson, P. Coppo, R. Frohlich, L. de Cola, A. van Dijken, M. Buchel, H. Borner, *Inorg. Chem.* **2007**, *46*, 11082.
33. Y. Mansoori, S. V. Atghia, S. S. Sanaei, M. R. Zamanloo, G. Imanzadeh, H. Eskandari, *Polym. Int.* **2012**, *61*, 1213.
34. SMART, *SAINT and SADABS*, Bruker AXS Inc., Madison, WI, **2012**.
35. G. M. Sheldrick, *SADABS v 2.03*, Göttingen, University of Göttingen, XXX, **2002**.
36. SHELXTL, *v 6.10*, Bruker AXS, Inc, Madison, WI, **2000**.

